SST-CFD Workshop March 1998

Validation and Evaluation of Turbulence Models for Aerospace Applications

D. SCHWAMBORN

Deutsches Zentrum für Luft- und Raumfahrt e.V.
Institut für Strömungsmechanik
Bunsenstraße 10, D-37073 Göttingen
Fax: +49 551 709 2416
email: Dieter.Schwamborn@dlr.de

Abstract

This paper deals with the evaluation of turbulence models done in the Numerical Methods Section of the Institut für Strömungsmechanik during the last years. This work covers subsonic, transonic and a few supersonic flows about 2D and 3D configurations. Examples discussed here include the transonic RAE2822 airfoil (cases 9 and 10), the ONERA Bump (case A and C) and the supersonic flow over a flat plate with a sharp fin. The turbulence models evaluated are algebraic or half-equation models, like the Baldwin-Lomax one with and without the Granville modification, the Johnson-King and Johnson-Coakley model, as well as the one-equation model of Spalart-Almaras (with the Edwards modification). Additionally a brief overview over results of other researchers on these test cases is given.

1 Introduction

In recent years CFD has become increasingly important in the development of new or advanced aircraft, since it allows in principle for an improved cost effectiveness of the design cycles and it provides information which is otherwise difficult to obtain, e.g. in a wind tunnel. Although the last decade has seen a tremendous progress in numerical algorithms, mesh generation, flow solvers and last but not least the computer power, the accurracy of numericals solution is still very much dependent on the physical modelling of transition and turbulence. Thus the validation of codes including the assessment of these models is an important prerequisite for the successful, i.e. accurate simulation of complex flow fields, as it is needed in the aircraft design and development.

Here we attempt to give an overview on our work (i.e. in the Numerical Methods Section of the Institute) with respect to the validation of turbulence models in the last few years. For quite some time the emphasis was on the more engineering type of model which was not too sophisticated and could therefore be routinely used in 2d and 3d aerodynamic calculations. Thus mostly algebraic or half-equation models have been used in our structured Navier-Stokes solvers. During the development of DLR's adaptive Navier-Stokes solver TAU-Code (Gerhold, 1996) for unstructured hybrid grids, however, more modern turbulence models were looked after. This led to the implementation of the Spalart & Almaras (1992) model including its variant due to Edwards & Chandra (1996). Since further models will be implemented only in the near future, we will supplement our own experience with a few results from other researcher which evaluated different turbulence models using the same test cases.

The test cases are choosen such that there exists a good experimental data base and a broad range of numerical results. As far as transonic flow is concerned, this led to two flows with separation and/or shock boundary-layer interaction which, although they are all two-dimensional, are quite challenging. All the necessary information on these cases can be found in the book about the European project EUROVAL (An European Initiative on Validation of CFD Codes (Haase et.al., 1992)). For further interesting test cases and

a concise description of numerous turbulence models see also the book on the European project ECARP (European Computational Aerodynamics Research Project: Validation of CFD Codes and Assessment of Turbulence Models, (Haase et.al., 1997)).

One three-dimensional example, a flow with swept shock-wave boundary-layer interaction, is presented, namely the supersonic flow over a flat plate with a fin (see e.g. Knight et.al. (1992)), where the standard Baldwin-Lomax model is compared to variants with engineering modifications (Panaras, 1996b).

2 Numerical Methods and Turbulence Models employed

The structured numerical method used in most of the calculations integrates the compressible, Reynolds-averaged Navier-Stokes equations with a finite volume Runge-Kutta method which is described in more detail in (Schwamborn, 1988) and (Kloppmann et al., 1994). The formulation is cell centered, and employs central fluxes across the cell faces with Jameson-type second and fourth order damping. A linearized four- or five-stage Runge-Kutta scheme is used to integrate the system of spatially discretized equations in time. The convergence to steady state is accelerated by a multi grid approach with local time stepping and implicit residual smoothing.

For the calculations with the Spalart-Almaras model the DLR TAU-Code (Gerhold et al., 1997)) was used, an adaptive Navier-Stokes solver for hybrid unstructured meshes based on a finite volume method operating on a dual grid. The code is of cell-vertex type, i.e. of cell-centered type with respect to the dual grid cell and employs various central and upwind schemes for the convective fluxes and an agglomeration multigrid approach for convergence acceleration. The adaptation feature of the code was, however, not used to obtain the results presented here, since the results for different models should be compared for the same mesh, if possible.

The turbulence models used in our calculations are not described here in detail, but instead the reader is refered to the original papers or to the fourth chapter of the ECARP Book (Haase et al., 1997), which gives a very concise, yet complete overview over many turbulence models from algebraic over one- and two-equation to Reynolds stress models. Here we only briefly discuss the modifications, if any, that we have made to the models or their constants.

The Baldwin Lomax (BL)

This model is used with two modifications compared to the original version. Instead of the original $C_{wk} = 0.25$ a value of 1.0 is used, resulting in that mainly the formulation $f_{wake} = y_{max} f_{max}$ is used in the outer viscosity formula. This leads to a more stable convergence of the numerical method at the expense of that the results for shock boundary-layer interaction deviate sometimes more from the experiment than with the original value. But the original value sometimes does not lead to a converged solution at all. Additionally, $C_{Kleb} = 0.52$ is used instead of 0.3, thus taking into account the findings of Stock & Haase (1987).

Furthermore we restrict the search for the location of the maximum moment of vorticity y_{max} to the vicinity of the wall ($y/c < const.$) to avoid unrealistic values outside the boundary layer. Once the position of f_{max} is found a quadratic fit is used to obtain the exact location of the maximum, i.e. $y_{max} f_{max}$. The transition criterion given for in the original BL model description is not used, i.e. we instantly switch the model on at a prescribed location.

The Granville Modification to the BL Model (GR)

Here we use the same modifications as given above except that we normally use the original $C_{wk} = 0.25$ and of course that the Klebanov constant is calculated by the model itself. To prevent C_{CP} from going to extremely high values the pressure gradient parameter β is not allowed to fall below -.112. In the wake of airfoil flow constant values C_{Kleb} and C_{CP} result from the fact that $u_\tau = 0$ at the wake center, i.e. we keep C_{Kleb} at a constant value of .45 resulting in a C_{CP} of 1.8.

The Johnson-King and Johnson-Coakley Model (JC and JK)

Here we use a time-dependent approach to the equations of the original papers, which was given by Abid et al. (1989) for a three-dimensional version of the original JK model and employ the BL model for the outer eddy viscosity formulation instead of the Cebeci-Smith model in the original approach. The advantage of this formulation is that it can be solved by an unsteady approach for all locations x along the surface without considering the local flow direction, which is not the case for a space-marching solution of the original formulation. Though the basic equations have been changed somewhat and the numerical approach to the

differential equation is made with a Runge-Kutta time-integration it is believed that the basic features of the JC and JK model are retained.

The Spalart-Almaras Model (SA)

The Spalart-Almaras model is used here only with the modification due to Edwards & Chandra (1996).

Before we come now to the test case a remark on compressiblity effects is certainly appropriate since most of the test cases are transonic and supersonic flows. It is believed, following Morkovin hypothesis that compressibility effects on eddies in wall-bounded flows are relatively small for Mach numbers below 5 (or even higher) and can, therefore, be neglected.

3 RAE2822 Airfoil

The RAE2822 airfoil test cases (Cook et al., 1979) are certainly among the most often calcutated transonic flows. Here we discuss the cases 9 and 10, which are flows with a shocks strenght that leads the turbulent boundary layer almost to separation or to incipient separation, respectively. Especially, case 10 is known to be difficult to compute with respect to the correct shock location and thus is a challenge for turbulence model validation. The calculations discussed in the following utilized structured grids (even for the hybrid TAU-Code for sake of comparison) of 257 by 65 nodes. Although an usually advisable mesh convergence study was not done here, two different meshes with different boundary layer resolution were used to gain at least a little insight in grid dependencies. Both meshes started from a smallest grid size normal to the wall of $y^+ = O(1)$, but showed a different resolution of the boundary layer and the difference in the results was found not to be essential for the general differences between the models discussed here (see the BL results in figures 1 to 3 and 4). For the influence of mesh size on e.g. the lift and drag see (Williams, 1994). Moreover it should be mentioned that we used the camber-corrected version of the airfoil shape and the correspondingly corrected flow parameters (Haase et.al.,1992).

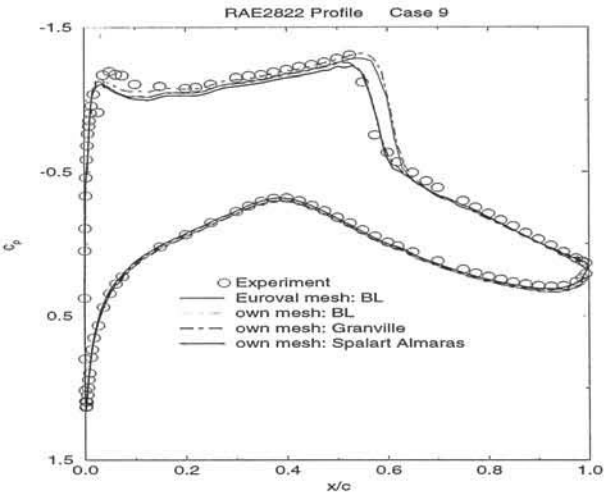

Figure 1: Pressure distribution for RAE2822-airfoil (case 9).

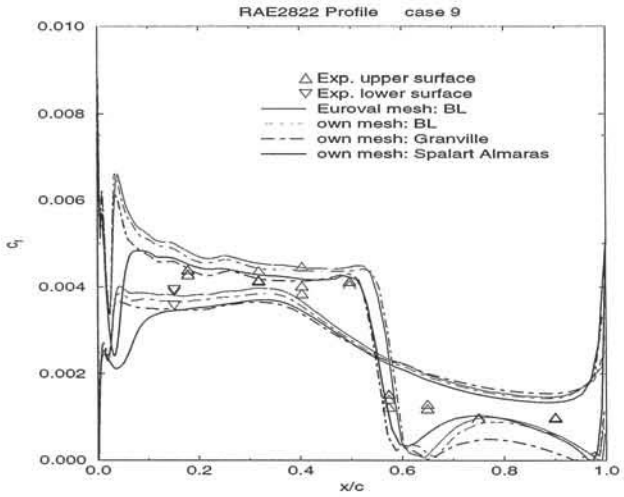

Figure 2: Skin friction distribution for RAE2822-airfoil (case 9).

Figures 1 and 2 show the pressure and skin friction distribution, respectively, for case 9 indicating that the BL model as used here is not able to predict a correct shock location, while the GR and the SA models perform well as do the JC and JK models, not shown here. It should be mentioned that the BL model will do a better job, when the numerically less stable original version with $c_{wk} = .25$ is employed. And the EUROVAL project mentioned above has shown that also the standard k-ε models work nicely for this test case. With respect to the transiton to turbulence it is noticed in both figure 2 and 4, that the immediate switching on of the algebraic models from one position to the other leads to a peak in the skin friction, while the SA model avoids this, due to its differential nature.

The situation changes, however, for case 10 depicted in figures 3 and 4. Now, the scatter between the methods becomes large and the GR model or the similarly behaving JC model (not shown here) show a too far downstream shock position. The same is true for the standard k-ε or k-ω model as can be seen in Menter

& Rumsey's (1994) results depicted in figure 5. Only the SA and Menter's k-ω-SST model predict almost the correct shock location. (Note that the difference in pressure level between figures 5 and 3 is probably due to application of the camber-correction in the results of the latter figure.)

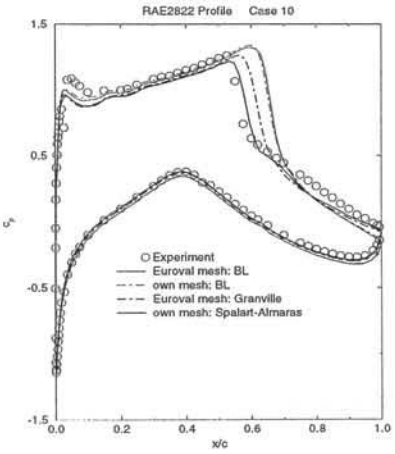

Figure 3: Pressure distribution for RAE2822-airfoil (case 10).

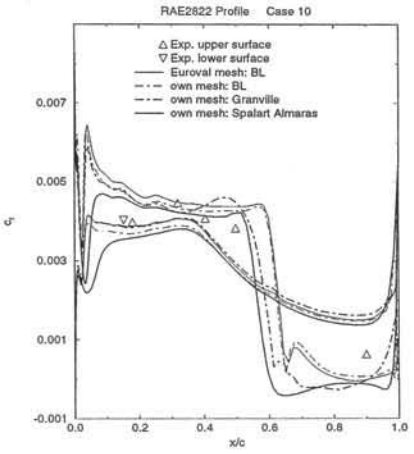

Figure 4: Skin friction distribution for RAE2822-airfoil (case 10).

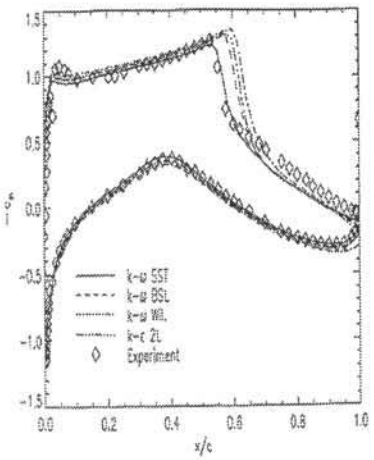

Figure 5: Pressure distribution for case 10 from (Menter, 1994) .

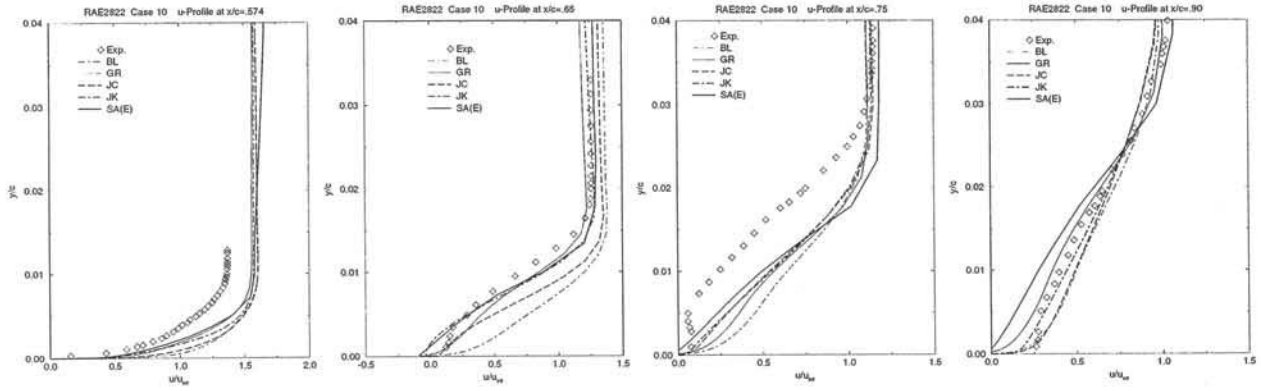

Figure 6: Velocity profile at
a) x/L = 0.574 b) x/L = 0.65 c) x/L = 0.75 d) x/L = 0.90

The velocity distributions at different locations normal to the upper airfoil surface (fig. 6) provide us with some more information on the model performance. Since all models used here produce a shock location which is at least a little bit too far downstream, none of the models matches the profile closest to the experimental shock position (a), while all models perform very good upstream of that position (not shown). Farther downstream (b) the agreement between the experiment and the SA, JK and GR models becomes good again except close to the wall where SA and JK predict already a little separation, i.e. GR is best, but with the wrong shock positon. It should, however, be mentioned that there is also some possible error in the experimental data, because skin friction could not be measured at positions a), b) and c) of figure 6.

The BL model does not even indicate incipient separation and the JC is in between BL and the others. At the next position (c) the discrepancies between the models become smaller again, but unfortunately none is close to the experiment, where the tendency to separation is even more pronounced without taking place. The same discrepancy was also found in the EUROVAL project for the one- and two-equation turbulence models (Haase et al., 1992). At the final station (d) the agreement between simulation and experiment is better again, with the SA result being farthest away from the experiment indicating that the SA model has some difficulty to recover from the separated flow situation.

4 Bump A and C

Although being internal flows (fig. 7), the Onera bump flow cases (Delery, 1981) offer a very good opportunity to validate models also for external flow. Unlike in the airfoil cases it is possible here by a careful adjustment of the downstream pressure to obtain the same shock position (in the inviscid part of the flow) in all numerical calculations as found in the experiment, without influencing the flow far upstream of the shock. Thus all models start from the same accelerated boundary layer which eases the comparsion quite a bit. The meshes for the calculations presented here are the mandatory meshes from the EUROVAL exercise (Haase et al., 1992) with a dimension of 193 by 65 and of 193 by 97 for case A and C, respectively.

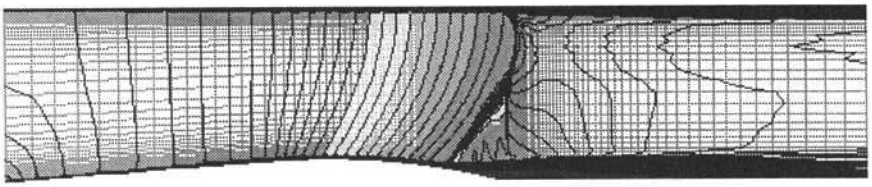

Figure 7: Bump C: Isolines of the Mach number for the bump C flow (computed with the TAU-Code and the SA model)

Case A is a flow with symmetric bumps on both upper and lower wall, such that a simulation of half the channel height is sufficient. The flow is adjusted with respect to the shock location along the symmetry plane, as can be seen from the distribution of the isentropic Mach number in figure 8. It is noticed, that the SA model is the only one to give the correct location of the shock together with a level of the exit pressure that is close to the experient. Figure 9 presents the corresponding result for the lower wall, indicating that all models perform correctly in the accelerated part of the flow up to the shock. The first discrepancy attracting the eye is certainly that in the level of the isentropic Mach number far downstream of the shock. This, however, can not be attributed to the flow simulation, but to some three-dimensional effects in the experiment farther downstream: as can be seen from a comparison of the experimental data in figures 8 and 9 there exists a pressure gradient across the chanel far downstream from the bump. Taking this necessary correction in exit pressure (and Mach number) into account, it is clearly the SA model which performs best, followed by the GR model. BL is worse with respect to the too steep decrease in Mach number, while the JC and especially the JK model show a tendency to a pressure plateau and a λ-shock which is not observed in the experiment.

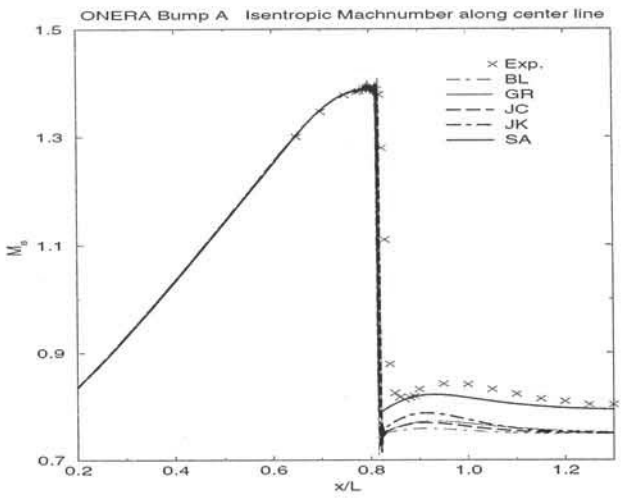

Figure 8: Bump A: Isentropic machnumber along centerline

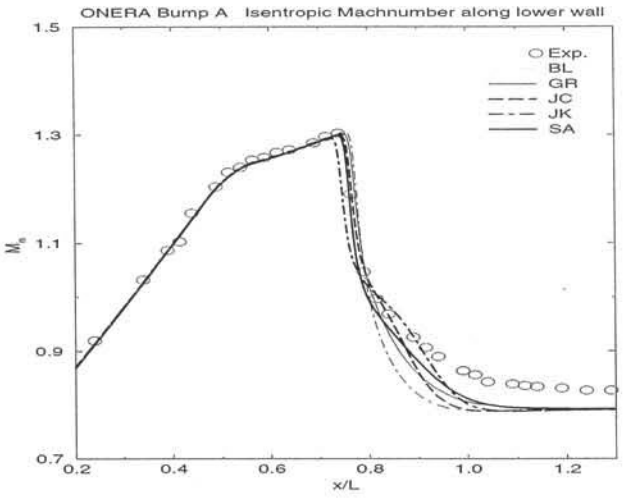

Figure 9: Bump A: Isentropic machnumber along lower wall

We change now to case C with the stronger shock boundary-layer interaction which leads to separation as can be seen from the λ-shock in the Mach isolines in figure 7. In figure 10 the upper wall isentropic Mach number is presented for this case. Although the interaction along this flat wall is not very strong we notice

qualitatively the same behaviour of the models as at the lower wall in case A. The good performance of the SA model is continued in the strong interaction region at the lower wall (fig. 11), where this model comes closest to the experiment if we take into account the downstream discrepancy due to the three-dimensionality of the experiment, also existing here. The JK model is the next closest to the experiment, followed by JC. Even the GR model indicates a tendency to a λ-structure, while the BL is unable to produce anything like that.

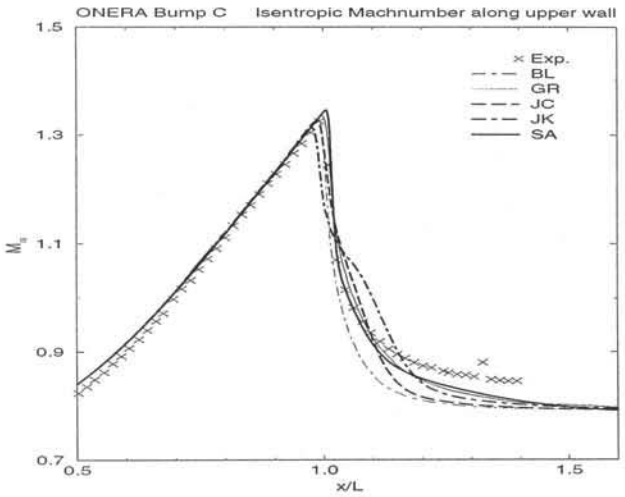

Figure 10: Bump C: Isentropic Mach number along upper wall.

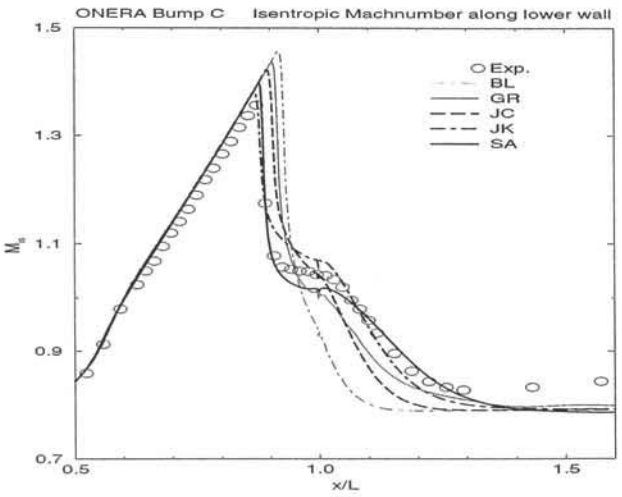

Figure 11: Bump C: Isentropic Mach number along lower wall.

To gain a little more insight in the model behaviour for this case we will briefly discuss the velocity profiles at some location just before and after the end of the bump (L=1.0). The good results of the SA model are found again in figure 12a) (somewhat downstream of the separation point) and figure 12b) (about the middle of the separation region). The JK model is not to far away as might have been expected and the JC and GR are about equal though with a larger discrepancy to the experiment. In figure 12c) (near the end of the separation), however, we find what we have already seen in the RAE2822 results: the SA model predicts still backflow and thus a much longer separation region, while the JK and GR models recover just in the right moment. Thus from the velocity profiles alone one would be tempted to judge the JK better than the SA, but one should not forget the tendency of the JK to predict a too strong shock boundary-layer interaction (λ-shock) which it not found in the experiment.

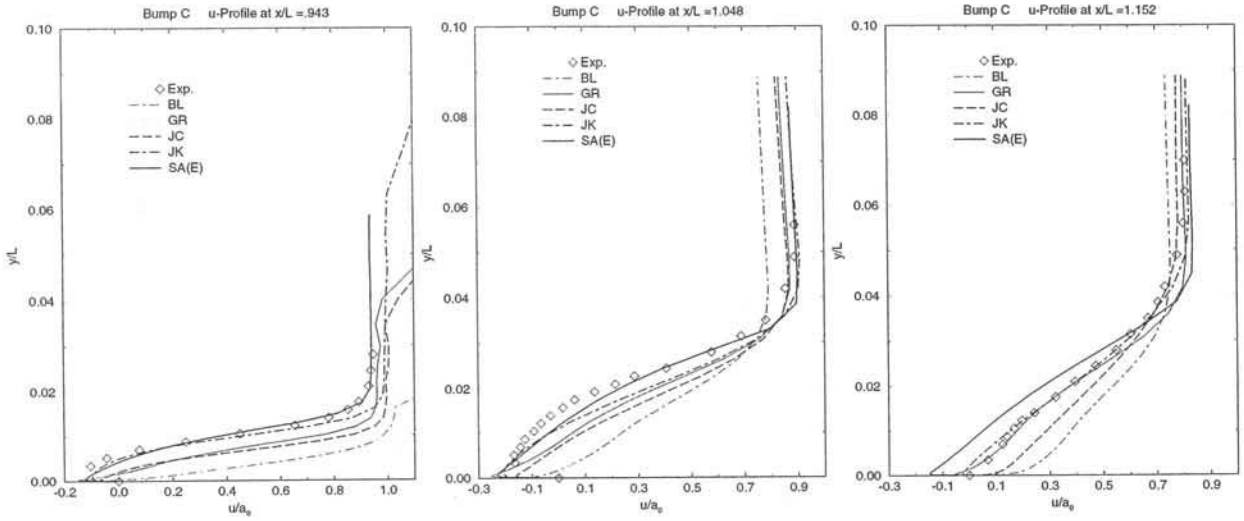

Figure 12: Velocity profile at

a) x/L = 0.940, b) x/L = 1.048, c) x/L = 1.152.

5 Sharp Fin

For the case of supersonic flow there exist a number of 3-D configurations which, despite of their simple geometry, reach a relatively high complexity of the shock-wave turbulent boundary layer interaction. Some of the most prominent, i. e. most extensively examined configurations (experimentally and numerically) are:

- the single sharp fin on a flat plate, see e.g. (Kim et al., 1990), (Knight et al., 1992), (Knight, 1993), (Lee et al., 1994), (Settles & Dodson, 1994), (Panaras,1996a), (Edwards & Chandra, 1996), (Panaras,1996b), (Knight, 1997);
- the symmetric or asymmetric crossing shocks, see e.g. (Knight, 1993), (Settles & Dodson, 1994), (Zha & Knight, 1996), (Knight et al., 1996), (Panaras,1996b), (Knight, 1997), and to a lesser extent
- the swept compression corner, see e.g. (Knight, 1993), (Settles & Dodson, 1994), and
- the cylinder with an offset cone, see e.g. (Knight et al., 1993), (Settles & Dodson, 1994), (Edwards & Chandra, 1996), (Knight, 1997).

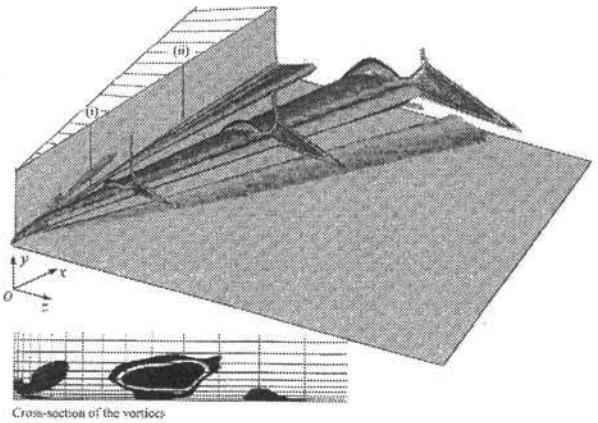

Figure 13: Sharp fin on flat plate configuration from (Panaras, 1996a).

Figure 13 shows an overview of the flow past the sharp fin on the flat plate, the case on which we will concentrate here. The shock wave produced by the fin interacts with the oncoming turbulent boundary layer on the plate and depending on the shock strength, i.e the Mach number and the wedge angle α, a quasiconical separation vortex under a λ-type shock structure is formed. This separation vortex transports high energy air from outside the boundary layer into the reattachment area leading to increased heat loads in that area. Panaras (1996a) found in his studies that at the same time the inner layers of the undisturbed boundary layer, where the eddy viscosity is high, wind around the core of the vortex. However, the outer layers, which have low turbulence, rotate over the vortex and penetrate into the separation bubble at the reattachment region forming a low-turbulence tongue, which lies along the plate, underneath the vortex. The intermittency of the air which constitutes the tongue, is very small, i.e. the flow is almost laminar there. At the initial stage of development the conical vortex is completely composed of turbulent air, but downstream, as it grows linearly, the low-turbulence tongue is gradually formed. Panaras found further that an increase of the strength of the interaction results in the folding around the vortex of purely inviscid higher layers. In the other extreme, in a weak interaction, a low-turbulence tongue is not formed. This behaviour makes this flow very interesting and difficult for the validation or calibration of turbulence models.

Panaras (1996a,b) uses the BL model with a modified wall distance $\eta = 2yz/(y+z+\sqrt{y^2+z^2})$ of (Hung & MacCormack, 1978) in order to account for the existence of two walls. After detailed numerical analysis of the sharp-fin flow at different Mach numbers and wegde angles α Panaras (1996b) found that the modification of the BL model due to Degani & Schiff (1986), which was introduced to account for the vortical flow, is not sufficient here. Thus he developed two modifications of the Baldwin-Lomax model which are based on a change in the wake function F_{wake} through the introduction of reference values for the maximum moment of vorticity (F_{max}) and its distance from the wall (y_{max}) outside the interaction region.

Since the derivation and the exact description of these modification would be too lengthy for this paper we refer the reader to (Panaras, 1996b). Here, we present only results for the case M=4.0, α =20 from the experiments of Settles & Dodson (1994). In figure 14 the pressure, skin-friction and wall flow angle are presented as obtained by Panaras (1996b) with the BL model and its two variants. Figure 15 taken from (Knight, 1997) shows results obtained with a Jones-Launder k-ε and the SA model of Edwards for comparison.

As one can see, the SA-E and the models of Panaras perform very good considering the pressure distribution compared to the standard BL or the k-ε model. For the flow angle the BL-P models are even better than the SA-E model. Concerning the skin-friction the situation is less clear: both SA-E and BL-P show a

peak which does not appear in the corrected experimental data as mentioned in (Knight, 1997), but in the experimental data of (Settles & Dodson, 1994). Although Panaras gives also an example for a crossing shock case (Panaras, 1996b) where his model 2 seems to work reasonably well, the major disadvantage of his models is their dependance on reference locations which have to be defined by the user. Thus a one-equation model like the SA-E model is much more attractive, as it seems to work quite well for a number of different situations without any user interference.

This is to a certain degree also true for other one-equation models of the Baldwin-Barth type. In (Edwards & Chandra, 1996) two BB modifications as well as the Edwards & McRae (1993) and the SA-E model are compared for a sharp-fin flow at Mach = 8 and for an offset cylinder-cone configuration at Mach 2.9, showing very good agreement with respect to the pressure distributions and at least resonable agreement for the skin-friction. The largest discrepancies are found for the heat transfer, which is somewhat in contrast of other results from sharp-fin calculations, see (Kim et al., 1990), (Knight, 1993), ((Lee et al., 1994), where the use of k-ε models (Jones-launder and Rodi type) results in quite good agreement between numerical simulation and experiment, even for the heat flux.

6 Conclusion

From what we have discussed in this paper one can draw a number of conclusions:

The BL model is not really worthwhile to be considered for computations in cases of non-equilibrium turbulence, like strong shock boundary-layer interaction, although it can perform well in near equilibrium cases of turbulence or even in non-equilibruium ones, if carefully tuned or modified as e.g in the fin test case. The Granville modification is usually considerably better, easy to implement and computationally cheap. Unfortunately, this is restricted to two-dimensional flow. Comparing the performance of the algebraic models with that of the half-equation models one might be tempted to always prefer the latter. Their complexity, however, is reasonably higher, one has always to produce an equilibrium solution first and they often tend to either overpredict shock boundary-layer interaction in near equilibrium cases (JK) or to underpredict it in more non-equilibrium cases (JC). Compared to these the newer one-equation models like Spalart-Almaras or Baldwin-Barth are not that much more complex or costly and should be considered instead. Although they have their own deficiencies as we have seen, e.g. with respect to recovery of the flow after separation in the case of the SA model, they perform quite nicely and can be solved together with the other differential equations of a Navier-Stokes solver, easily.

The latter is also true for the two-equation models, where only the computational cost is higher due to the additional equation. Here k-ω or k-τ should be considered, which allow for the implementation of the SST-correction (which is based on the Bradshaw assumption, that turbulent shear stress should be proportional to turbulent kinetic energy). The SST correction should certainly be used in all calculation with stronger adverse pressure gradients, because all k-ε type models fail otherwise similarly to the simple algebraic models.

7 Acknowlegement

The author gratefully ackowledges the help of his collegues at DLR (T. Gerhold and V. Hannemann) for providing results with the TAU-Code, which were obtained within the DLR projects MEGAFLOW and ADIF. Thanks are also due to Prof. A. Panaras, who provided the sharp fin results, which he obtained during his stay as a guest scientist, which was made possible through a grant from the CEC's Human Capital and Mobility Programme.

8 References

Abid, R., Vatsa, V.N., Johnson, D.A., Wedan, B.W., 1989, Prediction of Separated Transonic Wing Flows with a Non-equilibrium Algebraic model, AIAA paper 89-0558

Cook, P.H., McDonald, M.A., Firmin, M. C. P., 1997, Airfoil RAE2822- Pressure distributions, and boundary layer and wake measurements, AGARD-AR-138

Degani, D., Schiff, L.B., 1986, Computation of Turbulent Supersonic Flows around Pointed Bodies Having

Crossflow Separation. J. of Comput. Phys. 66, 173-196

Delery, J., 1981, Investigation of strong shock turbulent boundary layer interaction in 2D flows with emphasis on turbulence phenomena, AIAA paper 81-1245

Edwards, J.R., Chandra, S., 1996, Comparison of Eddy Viscosity-Transport Turbulence Models for Three-Dimensional, Shock-Separated Flowfields. AIAA J., Vol.34, pp756-763

Edwards, J.R., McRae, D. S., 1993, Nonlinear Relaxation Navier-Stokes Solver for Three-dimensional, High-Speed Internal Flows, AIAA J., Vol.31, No.7, pp1222-1228.

Gerhold, T., Galle, M., Friedrich, O., Evans, J., (1997), Calculation of Complex Three-Dimensional Configutrations Employing the DLR-TAU-Code, AIAA paper 97-0167

Goldberg, U.C., Ramakrishnan, S.V. 1993 A Pointwise Version of the Baldwin-Barth Turbulence Model. AIAA paper 93-3523

Haase, W., Brandsma, F., Elsholz, E., Leschziner, M. A., Schwamborn, D., 1993, EUROVAL - An European Initiative on Validation of CFD Codes. Notes on Numerical Fluid Mechanics, Vol. 42

Haase, W., Chaput, E., Elsholz, E., Leschziner, M. A., Mller, U. R., 1997, Validation of CFD Codes and Assessment of Turbulence Models. Notes on Numerical Fluid Mechanics, Vol. 58

Hung, C.M., MacCormack, R.W., 1978, Numerical solution of three-dimensional shock-wave and turbulent boudary-layer interaction, AIAA J., Vol16, No. 10, pp1090-1096

Kim, K.-S., Lee, Y., Alvi, F.S., Settles, G.S., Horstmann, C.C., 1990, Laser Skin Friction Measurements and CFD Comparison of Weak-to-Strong Swept Shock/Boundary- Layer Interactions. AIAA paper 90-0378

Kloppmann, Ch., Schwamborn, D., Singh, J.P., (1994), Multigrid Solution of the 2-D Navier-Stokes Equations for Transonic Internal and External Flows, in Contributions to Multigrid, CWI Tracts 103, CWI, Netherlands

Knight, D.D., Badekas, D., Horstmann, C.C., Settles, G.S., 1992, Quasiconical Flowfield Structure of the Three-Dimensional Single Fin Interaction. AIAA J., Vol.30, No. 12, pp2809-2816

Knight, D.D., 1993, Numerical Simulation of 3-D Shock Wave Turbulent Boundary Layer Interactions. AGARD R 792, paper No. 3

Knight, D.D., Garrison, T.J., Settles, G.S., Zheltovodov, A.A., Maksimov, A.I., Shevchenko, A.M., Vorontsov, S.S., 1995, Asymmetric Crossing-Shock-Wave/ Turbulent-Boundary-Layer Interaction. AIAA J., Vol.33, No. 12, pp2241-2249

Knight, D.D., 1997, Numerical Simulation of Compressible Turbulent Flows Using the Reynolds-Averaged Navier-Stokes Equations. R-819, paper No.5

Lee, Y., Settles, G.S., Horstmann, C.C., 1994, Heat Transfer Measurements and Computations of Swept-Shock-Wave/Boundary-Layer Interactions. AIAA J., Vol.32, 726-734

Menter, F.R., Rumsey, C.L., 1994, Assessment of Two-Equation Turbulence Models for Transonic Flows. AIAA paper 94-2343

Panaras, A.G., 1996a, The effect of the structure of swept-shock-wave/turbulent-boundary- layer interactions on turbulence modelling. DLR-IB 223-96 A21; also: J. Fluid Mech. 338, pp203-230, 1997

Panaras, A.G., 1996b, Algebraic Turbulence Modeling for Swept Shock-Wave/Turbulent Boundary-Layer Interactions. DLR-IB 223-96 A22; also: AIAA J., Vol.35, pp456-463,1997

Schwamborn, D., (1988), Simulation of the DFVLR-F5 Wing Experiment Using a Block Struktured Explicit Navier-Stokes Method. Notes on Numerical Fluid Mechanics, Vol. 22, pp244 - 268, Vieweg

Settles, G.S., Dodson, L.J., 1994, Supersonic and Hypersonic Shock/Boundary-Layer Interaction Database. AIAA J., Vol.32, No. 7, pp1377-1383

Spalart, P.R., Almaras, S.R., 1992,, A One-Eqation Turbulence Model for Aerodynamic Flows. AIAA paper 92-0439

Stock, H.W., Haase, W., 1987, The Determination of Turbulent Length Scalesin Algebraic Turbulence Models for the Navier-Stokes Method, AIAA J., Vol.27, No.1, pp.5-14

Williams, B.R., 1994, Computations of 2D Naiver-Stokes equations. GARTEUR/TP-067.

Zha, G.-C., Knight, D.D., 1996, Computation of 3D Asymmetric Crossing Shock Wave/Turbulent Boundary

Layer Interaction Using a Full Reynolds Stress Equation Turbulence Model. AIAA paper 96-0040

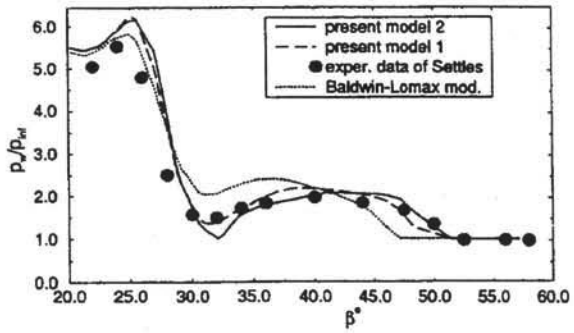

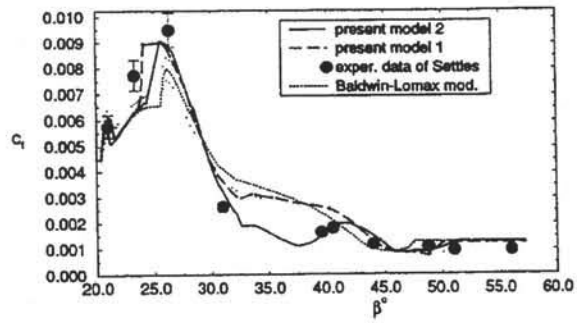

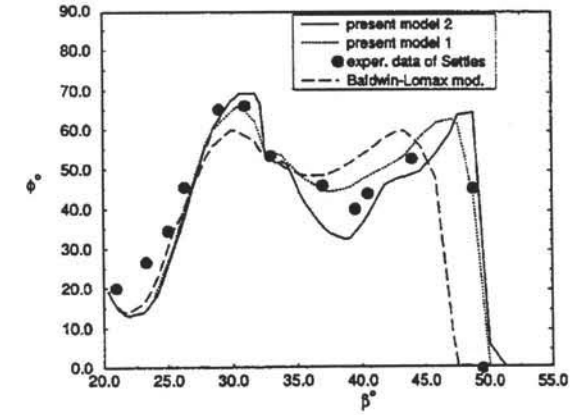

Figure 14: Pressure, skin friction and flow angle on the plate at a radius R = 101.6mm (Panaras, 1996a).

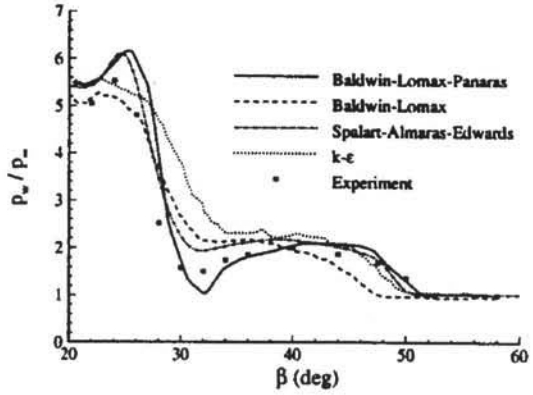

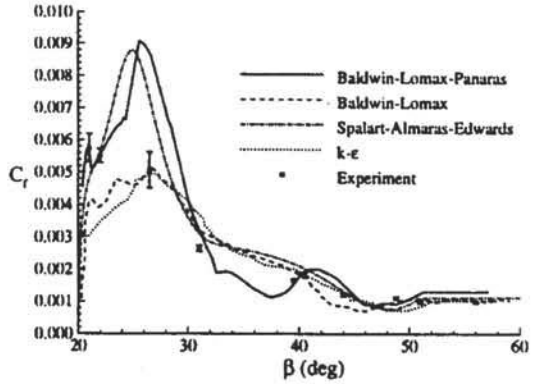

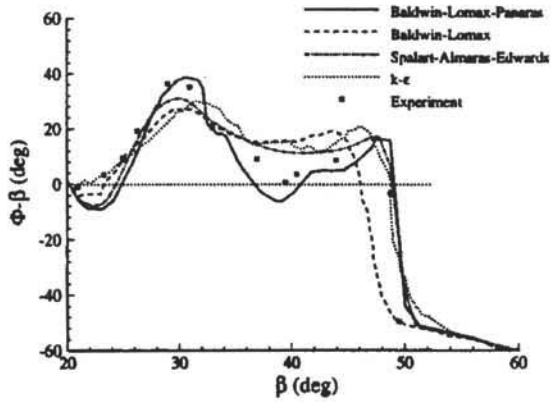

Figure 15: Pressure, skin friction and flow angle on the plate at a radius R = 101.6mm (Knight, 1997).